Phase Equilibrium Investigations of the Adirondack Class Basalts from the Gusev Plains, Gusev Crater, Mars

by

Anna Gabrielle Bogan Monders

B.A. Geology
Whitman College 1999

SUBMITTED TO THE DEPARTMENT OF EARTH, ATMOSPHERIC, AND PLANETARY SCIENCES IN PARTIAL FULFILLMENT OF THE REQUIREMENTS FOR THE DEGREE OF

MASTER OF SCIENCE IN GEOLOGY AND GEOCHEMISTRY
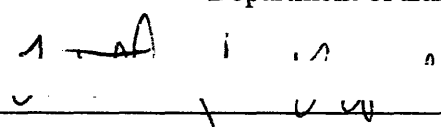
at the

MASSACHUSETTS INSTITUTE OF TECHNOLOGY
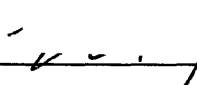
June 2006

Signature of Author_____
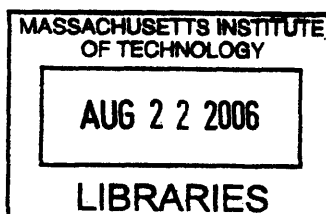Department of Earth, Atmospheric, and Planetary Sciences
May 12, 2006

Certified by_____
Timothy L. Grove
Professor of Geology
Thesis Supervisor

Accepted by_____
Maria T. Zuber
Department Head

Phase Equilibrium Investigations of the Adirondack Class Basalts from the Gusev Plains, Gusev Crater, Mars

by

Anna Gabrielle Bogan Monders

Submitted to the Department of Earth, Atmospheric, and Planetary Sciences on May 12, 2006 in partial fulfillment of the requirements for the degree of
Master of Science in Geology and Geochemistry

ABSTRACT

Phase equilibrium experiments have been performed on a synthetic analog of the Gusev plains basalt composition from the Spirit landing site on Mars, determined by the Alpha Particle X-ray Spectrometer on the Spirit Rover (Gellert *et al.*, 2006; McSween *et al.*, 2006). The near-liquidus phase relations were determined over the pressure range of 0.1 MPa to 1.5 GPa and at temperatures from 1105 °C to 1390 °C in a piston cylinder apparatus and 1-atm gas mixing furnace. The composition is multiply saturated with olivine, orthopyroxene, and spinel on the liquidus at 1310 °C and 1.0 GPa, or 85 km depth on Mars, placing an upper limit constraint on the thickness of the Martian lithosphere at the time of eruption. Experiments carried out at 0.1 MPa show Fo_{77} olivine as the first liquidus silicate mineral, appearing near 1250 °C. Olivine and spinel co-crystallize until pigeonite and plagioclase (An_{73}) join the crystallizing assemblage at 1125 °C. Low pressure crystallization of the Gusev composition does not produce liquids that could be parental magmas to surface types 1 and 2 of the Martian surface, nor do they appear to be related to olivine-phyric shergottites or other SNC meteorites. The iron-rich Gusev basalts appear to have been crystallized from a less depleted mantle source than the magnesian olivine-phyric shergottite Yamoto 980459.

Thesis Supervisor: Timothy L. Grove
Title: Professor of Geology

Table of Contents

List of Figures

List of Tables

Chapter 1

INTRODUCTION

Until recently the only information on the composition of igneous rocks on Mars and Martian magmatic processes came from SNC meteorites (McSween, 2002). With the exception of one ancient sample (ALHA84001, a pyroxenite cumulate), these meteorites are young magmatic rocks thought to have been ejected through meteoritic impact from the volcanic areas of Tharsis or Elysium. Most of these rocks contain accumulated crystals and therefore do not represent liquid compositions, and most are derived from evolved liquids that have experienced varying extents of fractional crystallization. Notable exceptions are several olivine shergottites (e.g., Yamato 980459, Greshake et al., 2004). Thus, it has been difficult to characterize Martian mantle processes and major element characteristics of Martian mantle source regions. Lavas were analyzed by the Mars Pathfinder mission using the Alpha Particle X-ray Spectrometer (APXS), but the analyzed compositions represent extremely evolved and differentiated andesitic magmas as well (Minitti and Rutherford, 2000).

Basaltic rocks have recently been described from the Spirit landing site at Gusev crater, and have been characterized as dark, fine-grained vesicular rocks, containing $\leq 25\%$ olivine megacrysts (McSween *et al.*, 2004; McSween *et al.*, 2006). Chemical analyses of abraded surfaces of these samples by APXS are consistent with primitive basalts, with an average of 11% MgO (McSween *et al.*, 2006). Gusev crater is located in the northernmost region of the highly cratered Southern Highlands and rocks with spectral characteristic similar to Gusev basalts have also been documented elsewhere in the Southern Highlands

(e.g., in the cliffs surrounding Isidis Planitia, Hoefen *et al.*, 2003), suggesting that this basalt composition may represent an important component of the ancient Noachian Martian crust.

In the following discussion, we will be concerned with the basalts from the floor of Gusev crater, analyzed during the first 155 sols of Spirit's mission before reaching the Columbia Hills. These basalts are represented by the rocks Humphrey, Adirondack, and Mazatzal, and have been classified by Squyres *et al.* (2006) as Adirondack Class. They will be referred to in this paper as Gusev basalts. We present the results of high-pressure, high-temperature phase equilibrium experiments on the Gusev basalts. The purpose of this study is to understand the formation conditions of these rocks, and we show that these basalts represent the first samples of near-primary magmas from Mars. On Earth, such primary basalts have been extensively used as the main tool to decipher melting conditions and thermal structure of the mantle (BVSP, 1981). Similarly, detailed study of the Gusev basalts could give information on mantle processes and melt generation on the early Mars. Low-pressure crystallization experiments are also utilized to determine the differentiation path of the Gusev basalts, and elucidate their relation to remotely sensed crustal compositions and shergottite-nakhlite-chassigny (SNC) meteorites.

Chapter 2

EXPERIMENTAL METHODS

2.1 Starting Materials

The starting composition for this study (Table 1) was a synthetic analog of the average of the published compositions for Adirondack, Humphrey and Mazatzal (McSween et al., 2006) based on the recalibrated APXS data (Gellert et al., 2006). An oxide mix was prepared using high-purity oxides (SiO_2, TiO_2, Al_2O_3, Cr_2O_3, Fe_2O_3, MnO, MgO, NiO), synthetic $CaSiO_3$, Na_2SiO_3, and $K_2Si_4O_9$, natural fluorapatite (Durango, Mexico) and Fe sponge (Lindsley et al., 1974). The oxides were ground under ethanol for 5 hours in an automatic agate mortar and pestle, Fe sponge was added and the mixture ground for a final hour.

2.2 Low-Pressure Experiments

Experiments were performed on the synthetic Gusev basalt analog composition at 0.1 MPa in a Deltech DT31VT rapid quench gas-mixing furnace. Oxygen fugacity was controlled at or near the quartz-fayalite-magnetite (QFM) buffer using mixtures of CO_2-H_2 gas with volumetric flow rates equal to or less than 0.1 ml/s. Oxygen fugacity was monitored using CaO-ZrO_2 electrolyte cells that were calibrated at the Cu-Cu_2O and Fe-FeO buffers. Temperature was measured using Pt-$Pt_{90}Rh_{10}$ thermocouples calibrated against the melting points of NaCl, Au and Pd on the IPTS 1968 temperature scale (Biggar, 1972).

0.04-0.05 g of the Gusev mix was pressed into a pellet with elvanol as a binder. The pellet was sintered to a 0.008" 7-9% FePt alloy loop designed to minimize the exchange of iron between the silicate charge and the wire loop (Grove, 1981). Experimental durations varied from 3 hours at near-liquidus conditions to 170 hours at the lowest temperatures investigated.

2.3 High-Pressure Experiments

Elevated pressure experiments were carried out between 0.8 and 1.5 GPa in a 0.5 inch end-loaded solid medium piston cylinder apparatus (Boyd and England, 1960). The piston-in technique of Johannes *et al.* (1971) was used. The sample was pressurized to 1.0 GPa (0.8 GPa for 0.8 GPa runs) at room temperature before the temperature was brought up to 865 °C at a rate of 100 °C/minute. Temperature was held constant at 865 °C for 6 minutes and the pressure was raised to the experimental pressure. Temperature was increased to the final experimental temperature at 50 °C/minute. Experiments were maintained at pressure and temperature for the duration of the run (Table 2), and they were quenched by turning off the power to the controller. For experiments above 1.0 GPa, the runs were pressure-quenched by reducing pressure to 0.8 GPa as the power was turned off (Putirka *et al.*, 1996).

About 10 mg of the starting mix was loaded into a graphite crucible with a graphite lid and placed in a platinum capsule that had been triple crimped, welded shut and flattened on one end. Graphite powder was packed in above and below the crucible (Elkins *et al.*, 2000) and the top of the outer Pt capsule was crimped and welded shut. The capsule was fitted in an alumina sleeve and positioned in the hotspot of a graphite furnace using MgO

spacers. $BaCO_3$ cells wrapped with Pb foil were used as the pressure medium. The pressure was calibrated against the reaction anorthite + gehlenite + corundum = Ca-Tschermakite (Hays, 1966), and is accurate to ± 50 MPa. $W_{97}Re_3$-$W_{75}Re_{25}$ thermocouples were used to monitor and control temperature, with no correction for pressure effects on thermocouple EMF. A 20 °C correction was applied to account for the temperature difference between the sample in the hotspot and the location of the thermocouple. This temperature difference was measured by offset thermocouples. The thermal gradient over the length of the sample is less than 10 °C (Wagner and Grove, 1997) and the temperature is thought to be accurate to ±10 °C.

The oxygen fugacity (fO_2) imposed by the graphite capsule in our piston cylinder experimental assembly has not been measured directly. Other experimentalists have estimated the intrinsic oxygen fugacity of similar piston cylinder assemblies (Watson, 1987; Brooker et al., 1998) and suggest conditions near the quartz-fayalite-magnetite (QFM) buffer or more reducing, ~QFM-1.

2.4 Analytical Methods

The experimental run products were analyzed with the 4- or 5-spectrometer JEOL 733 Superprobe electron microprobes at the Massachusetts Institute of Technology. An accelerating voltage of 15 kV and a beam current of 10 nA were used. A 2 μm diameter beam was used to analyze crystalline phases and a 10 μm beam was used for glasses. Quantitative analyses were obtained using the Armstrong (1995) CITZAF correction package, which uses the Duncumb and Reed atomic number correction, the Reed

fluorescence correction, and Heinrich's tabulation of mass-absorption coefficients. To

minimize Na loss, the element was counted for 5 seconds at the beginning of an analysis.

Other elements were counted for up to 40 seconds depending on abundance level. See

Gaetani and Grove (1998) for a discussion of analytical precision.

Oxide (wt%)	Recalibrated data	Experimental composition
SiO_2	45.57	46.04
TiO_2	0.55	0.50
Al_2O_3	10.51	10.60
FeO*	18.80	18.66
Cr_2O_3	0.63	0.74
MnO	0.42	0.42
MgO	10.97	11.12
CaO	8.05	7.95
Na_2O	2.35	1.75
K_2O	0.08	0.06
P_2O_5	0.59	0.56
FeS	0.83	--
Total	99.34	98.41

Table 1. Recalibrated data represents an average of the compositions of Humphrey, Adirondack, and Mazatzal reported in McSween et al. (2006). Experimental composition is the average estimated composition of piston cylinder runs from mass balance.

Table 2. Experimental conditions and products.

Run #	Pressure	Temp (°C)	Time (h)	Phases[a]	K_D ol/liq	K_D pyx/liq	K_D sp/liq	K_D pl/liq	Mg# gl	Mg# ol	Mg# pyx	Mg# sp	Ca# pl	ΣR^{2} [b]	ΔFe [c]
GUS-35	0.1 MPa	1105	170	ol (20) + pig (7) + pl (10) + sp (1) + gl (59)	0.31	0.27	2.13	0.79	0.35	0.64	0.67	0.21	0.70	0.35	0.26
GUS-34	0.1 MPa	1125	139	ol (18) + pig (<1) + pl (<1) + sp (2) + gl (78)	0.32		1.88	0.82	0.40	0.68		0.26	0.73	0.39	-0.12
GUS-33	0.1 MPa	1150	118	ol (18) + sp (2) + gl (78)	0.32		2.34		0.40	0.68		0.22		0.41	-0.77
GUS-36	0.1 MPa	1195	25	ol (11) + sp (2) + gl (85)	0.30		1.83		0.44	0.72		0.30		0.38	-0.34
GUS-31	0.1 MPa	1240	4.5	ol (1) + sp (1) + gl (95)	0.31		1.97		0.51	0.77		0.34		0.39	-0.86
GUS-32	0.1 MPa	1260	4	sp (1) + gl (97)			1.83		0.52			0.37		0.32	-1.51
GUS-28	0.8 GPa	1300	4.5	ol (3) + sp (1) + gl (95)	0.34		1.60		0.50	0.75		0.38		0.23	-1.05
GUS-29	0.8 GPa	1325	4.5	sp (1) + gl (97)			1.34		0.53			0.46		0.34	-3.75
GUS-21	1.0 GPa	1310	4	ol (3) + opx (<1) + sp (1) + gl (96)	0.35	0.30	1.35		0.50	0.74	0.77	0.42		0.20	-0.07
GUS-20	1.0 GPa	1330	3	sp (1) + gl (98)			1.40		0.51			0.43		0.23	1.16
GUS-16	1.0 GPa	1350	2	sp + gl											
GUS-25	1.2 GPa	1315	3.5	opx (9) + sp (1) + gl (88)		0.30	1.34		0.47		0.75	0.40		0.31	-2.05
GUS-24	1.2 GPa	1335	3.25	sp (1) + gl (97)			1.51		0.52			0.41		0.27	-1.40
GUS-23	1.2 GPa	1355	2.25	sp + gl											
GUS-17	1.2 GPa	1375	2.5	sp + gl											
GUS-18	1.2 GPa	1390	2	sp + gl											
GUS-27	1.5 GPa	1380	3	sp (1) + gl (97)			1.36		0.52			0.44		0.34	-3.32
GUS-26	1.55 GPa	1360	3	opx (2) + sp (1) + gl (96)		0.31	1.28		0.50		0.76	0.44		0.22	-0.87

[a] Abbreviations: *gl* glass; *ol* olivine; *pyx* pyroxene; *opx* orthopyroxene; *pig* pigeonite; *sp* spinel. Phase proportions calculated by mass balance.

[b] Sum of squared residuals from mass balance calculation

[c] Apparent loss or gain of FeO estimated as $((FeO_{calculated} - FeO_{starting\ material})/FeO_{starting\ material})*100$

13

Chapter 3

EXPERIMENTAL RESULTS

3.1 Approach to equilibrium

The experiments presented in this study are synthesis experiments where crystals and liquid formed from a starting material that consisted of an oxide mixture. Phase appearance temperatures have not been reversed, because previous experience indicates that synthesis experiments are sufficient for determining equilibrium phase appearance temperatures when >40% melt is still present (e.g., Grove and Bence, 1977).

An important prerequisite for the attainment of equilibrium is that the bulk composition of the charge remains constant. This was evaluated using the least-squares materials balance technique of Bryan *et al.* (1969). Phase proportions were estimated (Table 2) to identify the loss or gain of iron using the compositions of crystals and liquids produced in the experiments (Table 3). Fe loss or gain was very low, with experimental bulk compositions within 4 % of the composition of the starting material (and even within 2% for all but three experiments). The sum of squared residuals (ΣR^2, Table 2) indicates how well the experimental products represent the starting compositions. A value of 0.0 indicates a perfect fit, and all experiments have values below 0.4, indicating that a constant bulk composition has been maintained.

We used the mass balance results of the piston cylinder experiments to estimate the experimental bulk composition (Table 1), and these calculations indicated that our starting composition contained somewhat lower Na_2O than the Gusev composition. This difference in

Na was not corrected for, because we felt that the experimental composition was sufficiently close to that of the APXS analyses, which range from 2.09 to 2.62 (McSween *et al.*, 2006), and certainly within analytical uncertainties for Na by APXS. There was also some unavoidable loss of Na in the 0.1 MPa experiments, despite the low gas flow rates, and these losses come with the need to use long experimental durations to achieve exchange equilibrium between silicate crystals and melt. Tormey *et al.* (1987) and Grove and Juster (1989) discuss the trade-off in attempting to achieve equilibrium in 0.1 MPa gas mixing experiments.

Approach to equilibrium was evaluated following the criteria devised by Grove and Juster (1989). They carried out reversal experiments between coexisting pyroxene and liquid, which would be the slowest phases to equilibrate in our experimental study, and found that the time required to approach exchange equilibrium varies with temperature and degree of crystallinity. An approach to equilibrium is demonstrated by regular major-element partitioning between crystalline phases and liquid. The mineral-melt Fe-Mg exchange distribution coefficient (K_D^{Fe-Mg}) between olivine and melt and pyroxene and melt for the Gusev experiments are summarized in Table 2 using the analyses of experimental products presented in Table 3. The average K_D^{Fe-Mg} for olivine (K_D^{Fe-Mg} olivine = $[X_{Fe}^{ol}X_{Mg}^{liq}]/[X_{Mg}^{ol}X_{Fe}^{liq}]$) was 0.32 ± 0.02 (1$\sigma$ standard deviation), 0.30 ± 0.01 for orthopyroxene (opx). For spinel, the K_D^{Fe-Mg} for the 0.1 MPa experiments is 2.00 ± 0.20 and for the piston cylinder experiments it is 1.40 ± 0.11. The different values for the spinel K_D^{Fe-Mg} may relate to differences in ferric iron in the low and high pressure experiments (Table 4). Spinels in the high pressure experiments have an average of 2.90 wt% Fe_2O_3 based on mineral formula renormalizations, and the spinels in the 0.1 MPa experiments have 11.35

wt% Fe_2O_3. The single 0.1 MPa experiment with pigeonite large enough to analyze had a

K_D^{Fe-Mg} of 0.27. Although we cannot confirm that all elements approached equilibrium, the

consistent K_D^{Fe-Mg} values are an indication that minerals have established a Fe-Mg exchange

equilibrium with surrounding melt. The average plagioclase-melt Ca-Na exchange

distribution coefficient (K_D^{Ca-Na} plagioclase = $[X_{Ca}^{plag}X_{Na}^{liq}]/[X_{Na}^{plag}X_{Ca}^{liq}]$) for the two 0.1

MPa experiments with plagioclase was 0.80 ±0.02.

3.2 Experimental Results

A pressure – temperature phase diagram for the Gusev basalt composition is

presented in Figure 1 and representative compositions are given in Table 3. Cr-rich spinel is

the first phase to crystallize at all pressures investigated. Calculations using the MELTS

program (Ghiorso and Sack, 1995) indicate that spinel might be stable to very high

temperatures (up to 1535 °C). We did not, however, attempt to locate the spinel liquidus,

because spinel stability is highly dependent on oxygen fugacity and Cr_2O_3 content of the

starting material, which are not well constrained for the Gusev basalts. The first silicate to

crystallize is olivine (Fo_{77}) at 1250 °C. Olivine and spinel co-crystallize until 1125 °C, when

plagioclase (An_{73}) and pigeonite join the crystallizing assemblage. At 1125 °C, the charge

contains 18 wt% Fo_{68} olivine, with a 22 wt% total crystallinity. The liquid contains 50.5%

SiO_2, 13.1% Al_2O_3, and 6.4% MgO. Our lowest temperature experiment at 1105 °C

contained 20% Fo_{64} olivine, 7% pigeonite, 10% An_{70} plagioclase, and 1% spinel.

At 1.0 GPa and 1310 °C, the Gusev basalt composition is multiply saturated with Fo_{74}

olivine, orthopyroxene (Mg# 0.77), and chromium-rich spinel on its liquidus (Mg# = molar

[Mg/(Mg + Fe)]). At pressures above the 1.0 GPa multiple saturation point, orthopyroxene is the first silicate phase to crystallize after spinel. At 1.2 GPa, opx (Mg# 0.75) appears at 1315 °C, and at 1.5 GPa, opx of Mg# 0.76 crystallizes at 1360 °C. Below 1.0 GPa, olivine is the first silicate phase to crystallize, and at 0.8 GPa, Fo_{75} olivine appears at 1300 °C.

Monders et al. (2005) carried out an experimental investigation of the Gusev basalt composition initially reported by the Spirit Rover team (McSween et al., 2004). It was later discovered that the sensor heads on the two Mars Rovers had been switched and the calibrations used in APXS data reduction were incorrect. Experimental results for this initial composition are presented in Appendix 1 and show that the differences in composition between the two analyses result in small, but resolvable, differences in the conditions of multiple saturation (Figure 1A). Compared to the recalibrated composition, the multiple saturation point for the preliminary composition was at 1.1 GPa and 1360 °C, a consequence of the higher MgO in the preliminary composition. The saturating liquidus phases remained the same (olivine + opx + spinel).

3.3. Liquid line of descent

A low-pressure fractional crystallization calculation for the Gusev basalts has been carried out using the phase proportions and appearance sequence determined in the 0.1 MPa experiments. Calculated liquid lines of descent are plotted on Figure 2, together with experimental data, the bulk composition for Adirondack, Humphrey, and Mazatzal, and the liquid line of descent calculated by the MELTS program (Ghiorso and Sack, 1995).

The fractional crystallization model is based on the following crystallization sequence: 1% Cr-rich spinel crystallization, followed by 18% crystallization of 98% olivine and 2% spinel. When the MgO concentration in the liquid is down to 6.2 wt% (1125 °C for the 0.1 MPa experiments), the crystallization sequence encounters a reaction relationship: olivine + liquid → plagioclase + pigeonite + spinel. The appearance of pigeonite as a crystallizing phase means that the residual liquid has reached the olivine-pigeonite reaction boundary, placing olivine in a peritectic reaction with pyroxene + liquid (Grove and Juster, 1989). A small amount of olivine (4%) reacts back with the liquid while crystallizing 52% plagioclase, 51% pigeonite, and 1% spinel. The model was continued to 5.03 wt% MgO, close to the MgO content of our lowest temperature experiment (1105 °C). The model fits the general trend for all oxides (Figure 2), and has a particularly good fit for FeO*, Al_2O_3, CaO, and P_2O_5. The slight offset in TiO_2 (Figure 2f) may result from the simplifications in modeling spinel crystallization. The match between the fractionation model and the experimental data is worst for Na_2O and SiO_2 (Figures 2a,e). This is a result of the unavoidable sodium loss in our 0.1 MPa experiments, which results in lower Na_2O and higher SiO_2 in the residual liquids. If we correct the liquid composition for this sodium loss, the match between experiments and model in Figure 2 improves substantially.

Figure 2 also compares MELTS calculations with the experimental and model liquid lines of descent for the Gusev composition. Calculations have been performed for temperatures between 1600 and 1090 °C and 0.1 MPa pressure, with oxygen fugacity fixed at the QFM buffer. MELTS generally recovers the experimental compositions well when spinel and olivine are the only crystallizing phases, however, temperatures are offset by about 35 °C (Table 5). Spinel is present in the highest temperature experiment (1260 °C) and MELTS

indicates that spinel appears at 1535 °C as the liquidus phase. Fo_{77} olivine begins to crystallize near 1250 °C, but MELTS has it appear at a somewhat higher temperature and Fo content: Fo_{81} at 1275 °C. Once MELTS reaches 1165 °C (MgO = 6.85 wt%), it indicates that plagioclase (An_{67}) should appear, followed by the predicted crystallization of pigeonite at 1155 °C, and the general crystallizing trend no longer matches the experimental data. Plagioclase (An_{73}) and pigeonite in the experiments do not appear until 1125 °C (liquid MgO = 6.40 wt%). According to MELTS, clinopyroxene (cpx) begins to crystallize at 1130 °C, whereas no cpx had begun to crystallize by our lowest temperature experiment at 1105 °C. 59 wt% liquid remains in the low temperature experiment, although MELTS indicates that less than 15 wt% liquid should remain and that the solidus should be reached by 1090 °C. A comparison of the experimental results and the MELTS calculations are summarized in Table 5. The iron-rich residual liquid produced by this Martian composition are probably in a part of the compositional space that is not well modeled by MELTS.
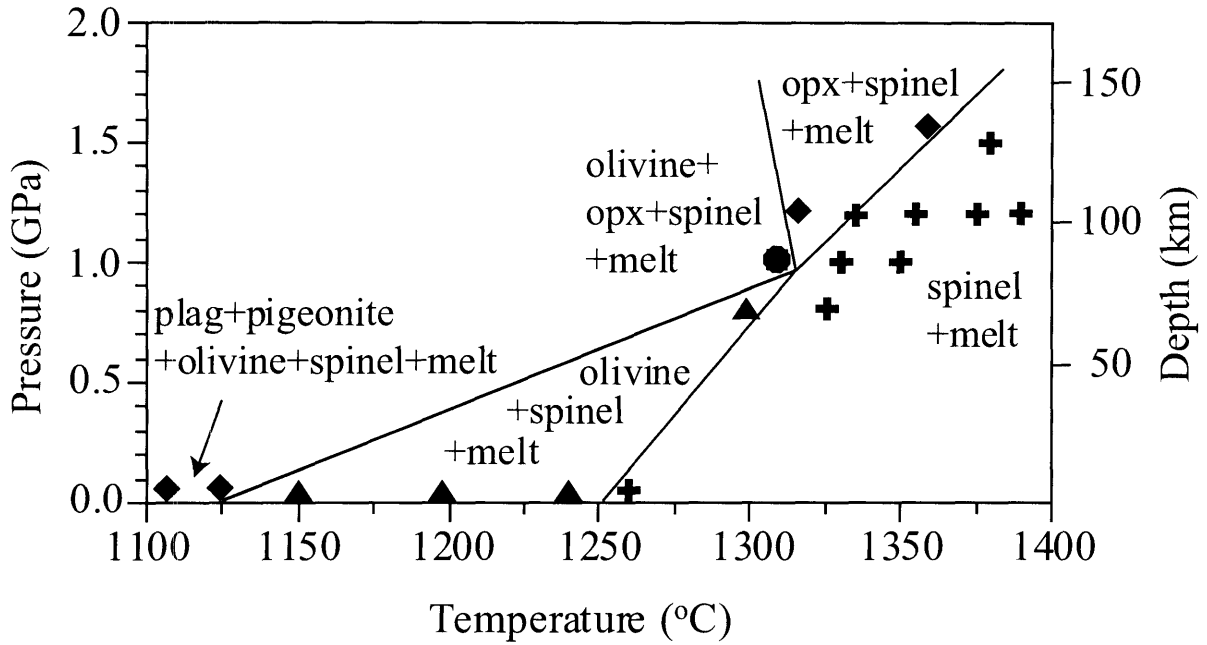
Figure 1. Experimental phase diagram for the recalibrated Gusev basalt composition. An olivine + orthopyroxene + spinel multiple saturation point was found on the liquidus near 1310 °C and 1.0 GPa (85 km depth).
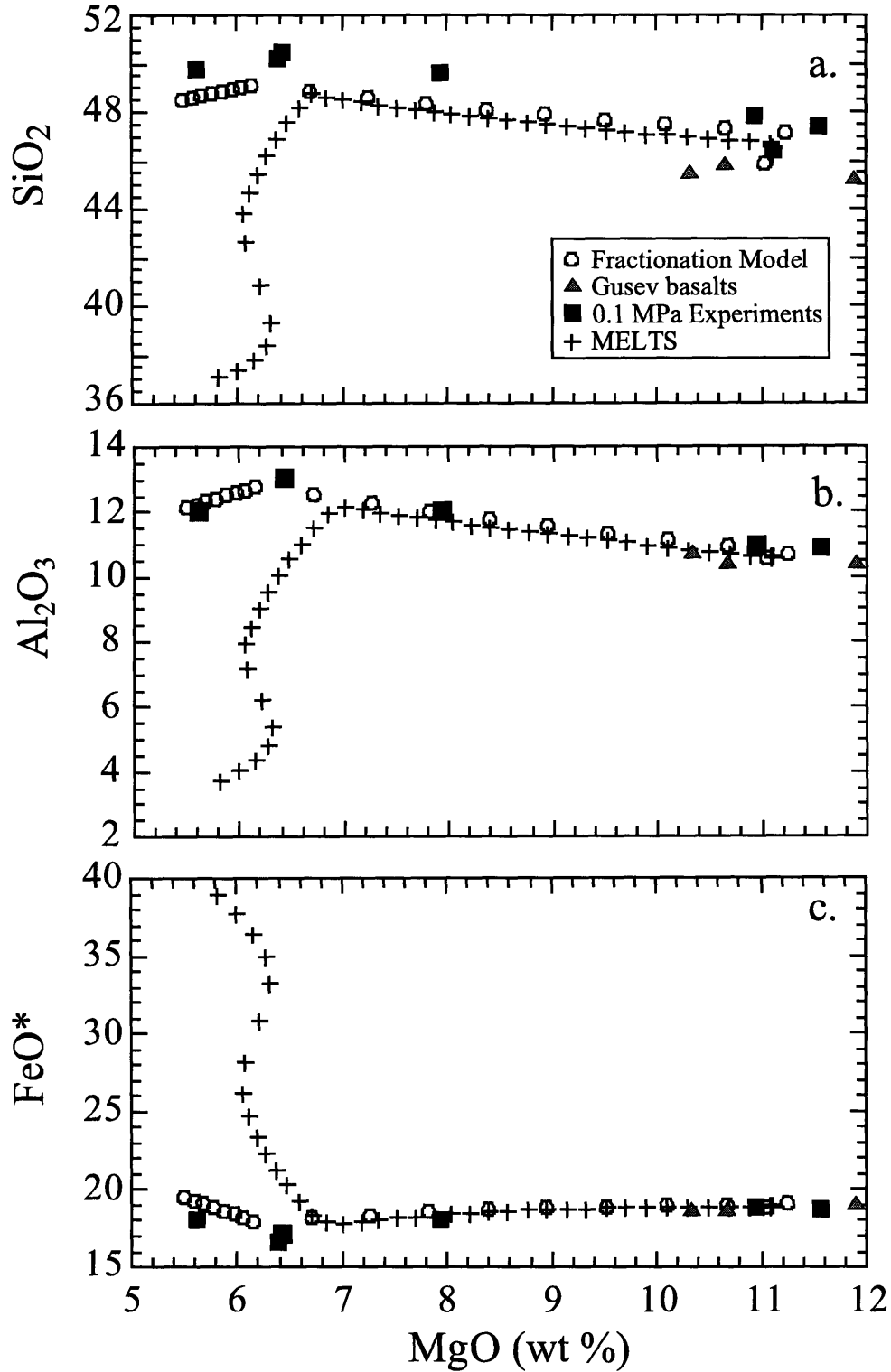
Figure 2. MgO vs. oxide data for eight oxides. The glass composition for the
0.1 MPa Gusev experiments are compared to the fractional crystallization model
presented in this paper and MELTS calculations for the recalibrated Gusev
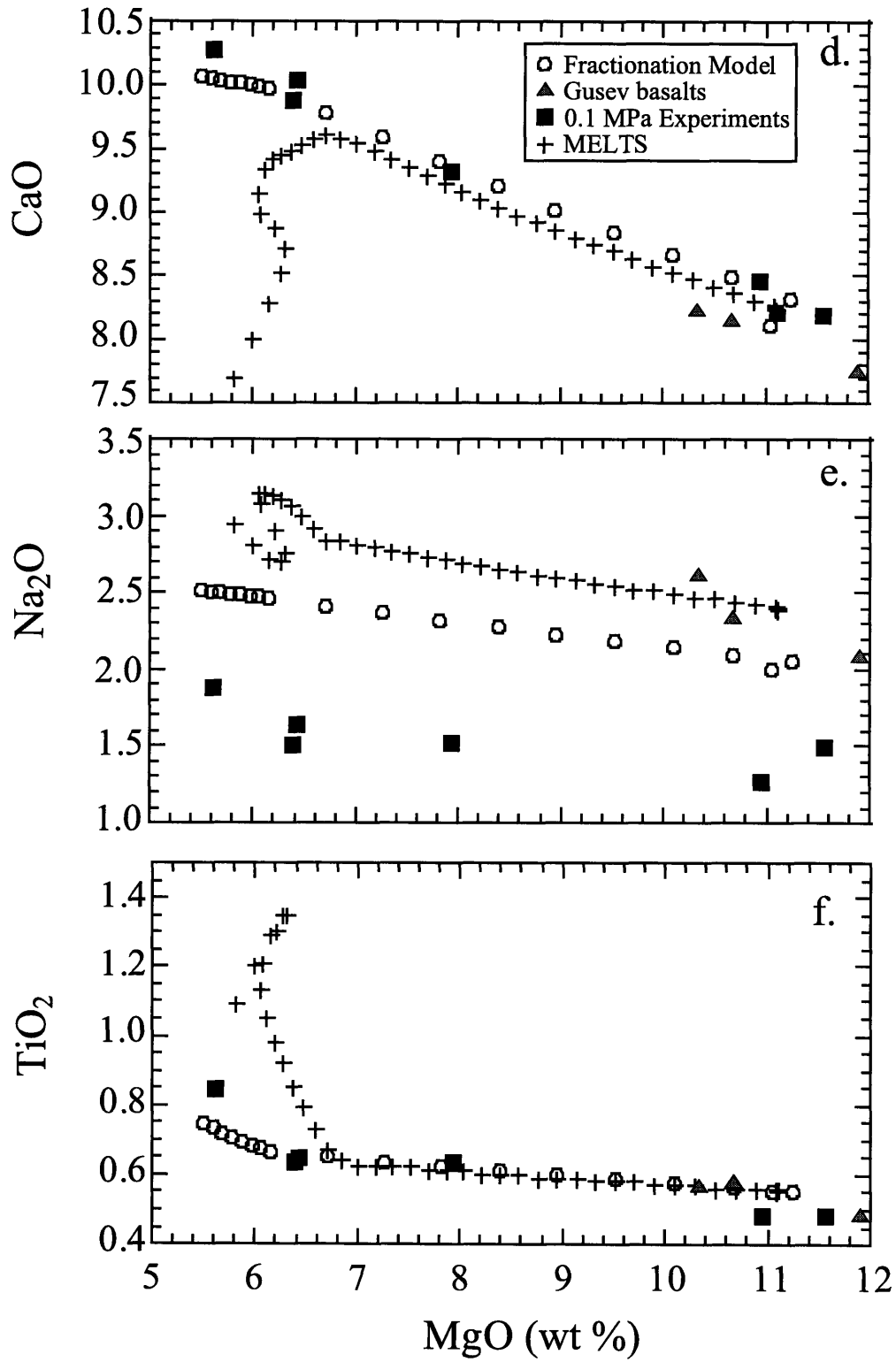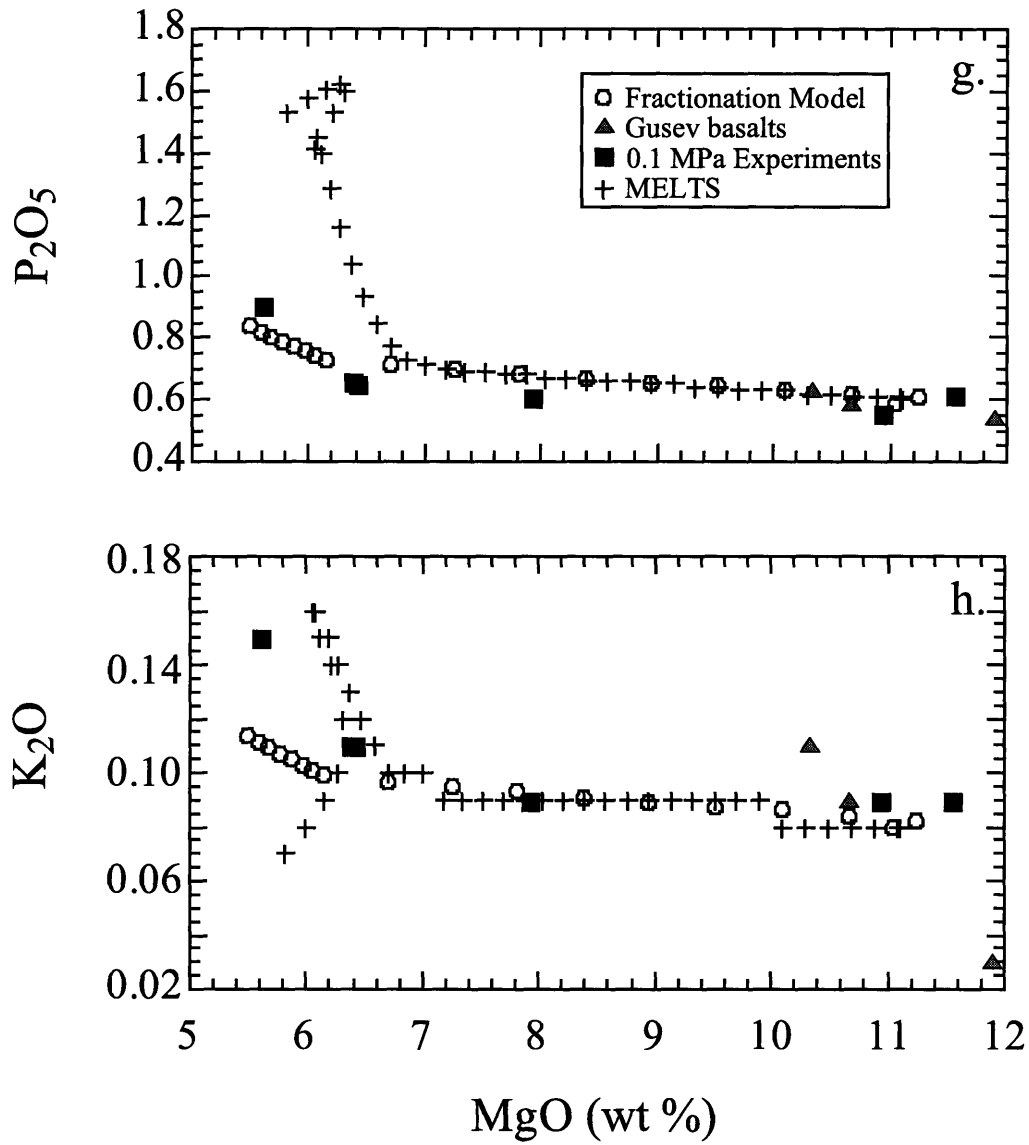composition.

Figure 2. (Continued from previous page)

Figure 2. (Continued from previous page)

Table 3. Electron microprobe analyses of phases produced in experiments

Run #	Phase[a]	SiO$_2$	TiO$_2$	Al$_2$O$_3$	Cr$_2$O$_3$	FeO	MnO	MgO	CaO	Na$_2$O	K$_2$O	P$_2$O$_5$	NiO	Total
0.1 MPa														
GUS-35	gl (10)[b]	49.9 (4)[c]	0.85 (7)	12.1 (1)	0.10 (7)	18.2 (2)	0.39 (3)	5.60 (20)	10.3 (1)	1.89 (11)	0.15 (1)	0.91 (8)		100.38
	ol (5)	36.8 (4)		0.07 (5)	0.13 (3)	31.4 (5)	0.61 (6)	30.7 (5)	0.43 (5)				0.05 (1)	100.22
	pig (9)	53.4 (4)	0.12 (3)	1.14 (31)	0.37 (6)	19.3 (1)	0.61 (2)	21.7 (5)	4.39 (3)	0.05 (3)				101.05
	pl (8)	50.8 (5)		30.3 (4)		1.35 (13)		0.29 (6)	14.3 (2)	3.34 (18)	0.03 (1)			100.39
	sp (8)	0.28 (11)	2.03 (19)	14.6 (1.0)	33.4 (2.0)	40.8 (9)	0.43 (4)	5.91 (12)	0.31 (4)					99.3[e]
GUS-34	gl (13)	50.5 (3)	0.65 (7)	13.1 (1)	0.04 (2)	17.2 (2)	0.36 (4)	6.40 (12)	10.1 (1)	1.65 (16)	0.11 (1)	0.65 (5)		100.80
	pig[d]													
	pl (7)	50.6 (8)		30.8 (5)		1.30 (14)		0.35 (7)	14.8 (4)	2.95 (20)	0.03 (1)			100.70
	ol (6)	36.7 (5)		0.09 (3)	0.16 (9)	28.4 (2)	0.55 (4)	33.2 (4)	0.38 (2)				0.10 (2)	99.62
	sp (4)	0.28 (12)	1.04 (1)	18.1 (5)	36.8 (3)	34.5 (3)	0.40 (4)	6.82 (13)	0.30 (3)					99.29
GUS-33	gl (11)	50.3 (3)	0.64 (7)	13.2 (7)	0.11 (3)	16.8 (2)	0.40 (2)	6.36 (10)	9.90 (16)	1.52 (11)	0.11 (1)	0.66 (7)		99.93
	ol (8)	36.6 (3)		0.06 (1)	0.10 (3)	28.1 (2)	0.57 (2)	33.6 (2)	0.31 (3)				0.08 (2)	99.34
	sp (4)	0.32 (3)	1.07 (7)	21.0 (2.1)	34.9 (2.1)	35.2 (5)	0.39 (3)	5.68 (95)	0.23 (9)					99.64
GUS-36	gl (11)	49.7 (2)	0.64 (6)	12.1 (1)	0.04 (2)	18.2 (2)	0.40 (3)	7.91 (8)	9.34 (7)	1.53 (12)	0.09 (1)	0.61 (5)		100.57
	ol (5)	37.3 (4)		0.06 (1)	0.11 (4)	25.5 (3)	0.13 (3)	36.5 (4)	0.35 (3)				0.03 (2)	100.00
	sp (4)	0.49 (25)	0.74 (25)	16.1 (7)	37.3 (1.7)	34.4 (1.1)	0.16 (5)	8.15 (39)	0.25 (5)					98.88
GUS-31	gl (10)	47.9 (3)	0.49 (6)	11.0 (1)	0.09 (7)	19.0 (3)	0.42 (4)	10.9 (2)	8.5 (1)	1.28 (7)	0.09 (1)	0.56 (4)		100.20
	ol (7)	38.0 (3)		0.06 (1)	0.12 (4)	21.4 (5)	0.41 (2)	39.3 (4)	0.26 (1)				0.11 (3)	99.70
	sp (5)	0.31 (17)	0.65 (5)	16.5 (4)	42.5 (4)	29.5 (3)	0.38 (4)	8.6 (8)	0.25 (5)					99.68
GUS-32	gl (10)	47.5 (2)	0.49 (10)	10.94 (4)	0.17 (2)	18.9 (2)	0.40 (4)	11.6 (2)	8.20 (10)	1.51 (9)	0.09 (1)	0.62 (1)		100.36
	sp (3)	0.33 (14)	0.57 (3)	16.2 (6)	43.2 (1.0)	28.7 (4)	0.35 (4)	9.99 (20)	0.30 (2)					100.64
0.8 GPa														
GUS-28	gl (10)	47.1 (3)	0.51 (7)	10.9 (2)	0.22 (7)	18.7 (3)	0.47 (6)	10.4 (2)	8.39 (8)	1.83 (14)	0.06 (1)	0.58 (12)		99.08
	ol (5)	37.7 (5)		0.06 (1)	0.22 (2)	22.8 (5)	0.42 (2)	37.5 (2)	0.25 (2)				0.02 (2)	99.00
	sp (3)	0.68 (10)	0.48 (2)	17.0 (3)	48.7 (3)	24.2 (1)	0.37 (4)	8.41 (47)	0.15 (7)					100.23

24

Table 3. (Continued from previous page)

Run #	Phase	SiO_2	TiO_2	Al_2O_3	Cr_2O_3	FeO	MnO	MgO	CaO	Na_2O	K_2O	P_2O_5	NiO	Total
GUS-29	gl (10)	47.3 (3)	0.45 (4)	10.7 (1)	0.32 (6)	18.5 (4)	0.41 (3)	11.6 (2)	8.14 (7)	1.86 (13)	0.05 (1)	0.59 (9)		99.88
	sp (4)	0.83 (38)	0.44 (2)	16.1 (7)	49.9 (6)	22.1 (2)	0.30 (4)	10.4 (4)	0.30 (10)					100.62
1.0 GPa														
GUS-21	gl (11)	46.6 (3)	0.54 (10)	11.0 (1)	0.25 (4)	18.7 (2)	0.44 (4)	10.4 (1)	8.45 (9)	1.93 (13)	0.063 (5)	0.67 (11)		99.13
	ol (7)	37.3 (2)		0.06 (2)	0.21 (2)	23.6 (2)	0.41 (3)	37.3 (2)	0.28 (2)				0.03 (3)	99.16
	opx (10)	53.6 (2)	0.04 (2)	2.52 (7)	1.09 (5)	14.3 (2)	0.35 (4)	26.6 (3)	1.52 (10)	0.09 (5)				100.09
	sp (4)	1.2 (1)	0.47 (2)	20.5 (1.2)	44.2 (9)	23.3 (6)	0.38 (3)	9.6 (5)	0.33 (6)					100.20
GUS-20	gl (13)	46.6 (2)	0.42 (6)	10.5 (1)	0.27 (4)	19.3 (1)	0.44 (3)	11.4 (1)	8.06 (12)	1.82 (14)	0.07 (1)	0.56 (5)		99.52
	sp(4)	0.39 (15)	0.41 (1)	18.1 (2)	47.0 (1)	23.3 (3)	0.34 (3)	9.82 (11)	0.21 (2)					99.96
1.2 GPa														
GUS-25	gl (10)	46.5 (3)	0.61 (7)	11.5 (1)	0.27 (3)	19.0 (2)	0.42 (5)	9.44 (22)	8.77 (10)	1.86 (20)	0.06 (1)	0.64 (9)		99.11
	opx (9)	53.5 (2)	0.07 (1)	3.16 (7)	1.20 (4)	15.2 (4)	0.35 (4)	25.5 (2)	1.73 (8)	0.09 (2)				100.75
	sp (4)	0.64 (23)	0.46 (1)	21.1 (3)	42.2 (5)	24.8 (7)	0.39 (3)	9.20 (34)	0.26 (4)					99.33
GUS-24	gl (12)	46.9 (3)	0.53 (4)	10.5 (2)	0.32 (4)	18.8 (3)	0.42 (4)	11.3 (2)	7.96 (10)	1.71 (11)	0.06 (1)	0.54 (6)		99.10
	sp (3)	0.47 (7)	0.42 (2)	17.8 (1.5)	47.7 (2)	23.4 (4)	0.36 (3)	9.30 (40)	0.23 (3)					99.97
1.5 GPa														
GUS-26	gl (9)	46.7 (2)	0.55 (5)	10.79 (7)	0.34 (3)	18.9 (2)	0.38 (2)	10.69 (9)	8.22 (9)	1.85 (7)	0.06 (1)	0.57 (8)		99.11
	opx (10)	53.2 (4)	0.03 (1)	2.85 (45)	1.29 (17)	14.8 (2)	0.08 (2)	26.6 (3)	1.50 (8)	0.09 (2)				100.41
	sp (5)	0.34 (8)	0.38 (2)	20.8 (6)	43.5 (9)	23.8 (4)	0.11 (2)	10.5 (3)	0.17 (2)					100.09
GUS-27	gl (11)	47.0 (3)	0.52 (9)	10.5 (1)	0.53 (3)	18.4 (2)	0.42 (4)	11.2 (2)	8.01 (8)	1.70 (10)	0.05 (1)	0.55 (5)		99.04
	sp (3)	0.34 (16)	0.36 (3)	17.1 (7)	49.7 (1.6)	22.5 (4)	0.27 (14)	10.1 (5)	0.22 (2)					100.84

[a] Abbreviations for phases are in Table 2

[b] Number of microprobe analyses

[c] One standard deviation of replicate analyses in terms of least unit cited. Thus 49.9 (4) should be read as 49.9 ± 0.4

[d] Pigeonite observed in GUS-34 but crystals too small to analyze

[e] Spinel totals summed using FeO and Fe_2O_3 values reported in Table 4

Run #	Fe_2O_3	FeO
0.1 MPa		
GUS-35	16.1	26.3
GUS-34	10.9	24.7
GUS-33	8.9	27.2
GUS-36	13.2	22.4
GUS-31	8.9	21.5
GUS-32	10.1	19.6
0.8 GPa		
GUS-28	1.7	22.7
GUS-29	2.6	19.8
1.0 GPa		
GUS-21	1.6	21.9
GUS-20	3.5	20.1
1.2 GPa		
GUS-25	3.5	21.6
GUS-24	2.7	21.0
1.5 GPa		
GUS-26	4.6	19.7
GUS-27	3.0	19.8

Table 4. Fe_2O_3 and FeO estimates for spinels based on charge balance

Phase Appearance	MELTS	0.1 MPa Experiments
Spinel	1535 °C	above 1260 °C
Olivine	1275 °C Fo_{81} Liquid MgO = 10.9	1250 °C Fo_{77} Liquid MgO = 10.9
Plagioclase	1165 °C An_{67} Liquid MgO = 6.85	1125 °C An_{73} Liquid MgO = 6.40
Pigeonite	1155 °C Liquid MgO = 6.58	1125 °C Liquid MgO = 6.40
Clinopyroxene	1130 °C Liquid MgO = 6.12	below 1105 °C
Solidus	1090 °C	59% liquid remaining in lowest temperature (1105 °C) experiment

Table 5. Comparison of MELTS calculations for the recalibrated Gusev composition and the 0.1 MPa experiments at QFM.

Chapter 4

DISCUSSION

4.1 High-Pressure Phase Relations

If a primary basaltic magma segregated from its mantle residue at a given pressure (P) and temperature (T), it should be multiply saturated on its liquidus with all the residual mantle phases (usually olivine + orthopyroxene ± clinopyroxene ± spinel) at P and T. Conversely, if a basaltic magma is multiply saturated with mantle phases at one P, T point on its liquidus, it can be argued to represent a primary mantle magma, and the pressure and temperature of the multiple saturation point will indicate the pressure and temperature of segregation (e.g. BVSP, 1981). The Gusev basalt composition is multiply saturated with opx + olivine + spinel at 1.0 GPa and 1310 °C. Opx and olivine near the multiple saturation point (Tables 2, 3) are enriched in FeO compared to terrestrial mantle minerals (olivine Fo_{74} and opx En_{77}, compare to BVSP, 1981). However, it is generally agreed that the Martian mantle is enriched in FeO compared to the Earth's mantle (e.g., Dreibus and Wänke, 1985; Halliday *et al.*, 2001). The experimental results thus suggest that the Gusev basalt is a primary to near-primary melt that segregated from the Martian mantle at 1.0 GPa and 1310 °C.

The composition of the Martian mantle has been estimated by Dreibus and Wänke (1984, 1985, hereafter referred to as DW), based on the composition of SNC meteorites and cosmochemical constraints. Bertka and Holloway (1994a, b) conducted a series of anhydrous experiments on the DW mantle composition, and determined phase relations and melt compositions from 1.0 to 3.0 GPa (Figures 3, 4). The olivine + opx + spinel multiple

saturation point obtained for the Gusev basalts falls very near the olivine + opx + spinel + liquid field determined for the DW primitive Martian mantle composition (Figure 3). Furthermore, composition of olivine and orthopyroxene at the multiple saturation point (Table 2) are similar to the composition of residual phases from melting experiments on the DW Martian mantle composition (Bertka and Holloway, 1994a). This provides additional support to the idea that the melts that formed the Gusev basalts were primary or near-primary magmas from the Martian mantle. Finally, this conclusion is also supported by comparison of the Gusev basalts and the melt composition from the DW Martian mantle (Bertka and Holloway, 1994b). Figure 4 shows a multiple oxides vs. MgO plot for glasses analyzed in their 1.5 GPa experiments done over a temperature range from 1300 to 1550 °C. The bulk compositions of Adirondack, Humphrey, and Mazatzal are consistent with experimentally determined melting compositions. According to Bertka and Holloway's (1994b) experiments, the melt fraction necessary to produce the Gusev basalts would be about 15 to 20%.

It has been argued that the Dreibus and Wänke (1985) estimate does not represent the composition of the Martian mantle, and other compositions, some of them very different, have been proposed (e.g., Sanloup et al., 1999; Agee and Draper, 2004). However, the results presented above make a coherent picture, and key characteristics of the Gusev basalts are incompatible with these other mantle compositions. For example, the pyroxene-rich composition proposed by Sanloup et al. (1999) is unlikely to produce olivine-rich basalts when melting, and the high-Mg, high $CaO / Al2O3$ source proposed by Agee and Draper (2004) is unlikely to produce the high-Fe, low $CaO / Al2O3$ Gusev basalt. Phase relations

and composition of the Gusev basalts thus support the Dreibus and Wänke (1985) estimate of the composition of the Martian mantle.

Two types of melting processes that might have led to the production of the Gusev basalts are batch melting and near-fractional adiabatic decompression melting (Kinzler and Grove, 1992). Batch melting would most likely occur during heating of lithosphere and decompression melting would happen in a convectively ascending mantle melt column; on Earth this process occurs at mid-ocean ridges.

The 1.0 GPa multiple saturation pressure is consistent with a batch melting process that formed the Gusev basalts in the Martian mantle at a depth of about 85 km. This places an upper limit constraint on the thickness of the Martian crust and mantle lithosphere in this area at the time of eruption. Age estimates of the Gusev basalt from crater counting are Late Noachian (3.65 Ga, Greeley *et al.*, 2005). Therefore, the early Martian lithosphere beneath the Gusev site was thin and mantle conditions allowed melting to occur. The current average thickness of the Martian crust is 50 km (Zuber *et al.*, 2000) and the estimate from experiments is in good agreement with this present day estimate. The temperature of multiple saturation, 1310 °C, is within the range that exists at Earth's modern mid-ocean ridges (1280 to 1475 °C (e.g. Kinzler and Grove, 1992; McKenzie and Bickle, 1988), indicating that conditions for Martian basalt production would be characterized by high mantle potential temperatures, similar to those on modern Earth. Greeley *et al.* (2005) suggest that the basalts emplaced on the floor of Gusev crater may be temporally related to volcanic activity on the southern side of Apollinaris Patera and may be the result of regional volcanism around 3.65-3.76 Ga.

If melting occurred by near-fractional adiabatic melting, the depth of multiple

saturation represents an average depth (or pressure) of melting. In near-fractional adiabatic

decompression melting, small melt increments (~ 1 % melting for 0.1 GPa of upwelling) are

produced and continuously separated from the mantle residue. As convecting mantle

ascends, it crosses the solidus and begins to melt. At the top of the melting column the

fractional melt increments are blended and the resulting aggregate melt represents the

average of the melts produced. The multiple saturation point of this aggregate melt also

gives an average pressure of melt generation. The Gusev basalts represent about 15 to 20 %

melting of a DW mantle, so the melting interval in the Martian mantle would be 0.75 to 1

GPa or 64 to 85 km long melting columns. For a 15 % melt with an average depth of

generation of 85 km, melting would begin at 140 km depth and end at 20 km depth. For a 20

% melt, melting would begin at 170 km depth and end at the surface. Adiabatic near

fractional melting would therefore require a thin lithosphere in the vicinity of melt

production of the Gusev basalts. Compositional features preserved in the major elements of

modern ocean floor basalts (especially Na_2O and FeO abundances) allow fractional vs. batch

melting to be distinguished (Kinzler and Grove, 1992). For an equivalent extent of melting,

fractional melts would be higher in Na_2O and FeO than batch melts. The close

correspondence between the Na_2O and FeO content of the DW melts (Figure 4) and the

Gusev basalts are consistent with a batch melting origin.

Other possible scenarios for batch melting that seem compatible with the geological

evolution of Mars include: (1) Generation above a mantle plume related to the Elysium

volcanic area, and (2) Generation very early in Mars' history, when the planet was not yet

cooled from early accretionary and impact processing heating and decay of short-lived

radiogenic isotopes. The strong contrasts with SNC meteorites (see 4.2.2. below), however, make this first option improbable. In the second case, Gusev basalts would be part of a primary basaltic crust, and their strong geochemical differences from SNC meteorites would be explained by the sampling of a different, primitive, relatively undifferentiated mantle.

Spectroscopic measurements have shown that most of the Southern Highlands are covered by rocks of basaltic composition (e.g. Christensen *et al.* 2000). Olivine has been identified by visible / near-infrared reflectance spectrometry (OMEGA investigation on board the Mars Express spacecraft, Mustard *et al.*, 2005) and thermal emission spectrometry (TES on board the Mars Global Surveyor spacecraft, Hoefen *et al.*, 2003; Hamilton and Christensen, 2005). It is thus possible that olivine-basalts similar to the Gusev basalts are representative of at least part of the Noachian Southern Highlands crust, an idea reinforced by their sampling a relatively primitive mantle source. If this is the case, the parameters derived from the Gusev basalts (lithospheric thickness, mantle temperature, melt fraction) can be used in geophysical models of the formation of the Noachian crust.

4.2 Low-Pressure Crystallization

4.2.1 Olivine Megacrysts

There is debate whether the olivine megacrysts observed in Adirondack, Humphrey, and Mazatzal are actual phenocrysts that crystallized *in situ* or represent an accumulation of crystals by settling in the lower portion of the cooling unit. (McSween *et al.*, 2006). McSween *et al.* (2004, 2006) propose that olivine accumulation might not have occurred and

that the basalt composition represents a liquid composition, based on the evidence that the rocks at the Gusev site have similar compositions despite differences in texture and modal olivine. Crystal settling in a lava flow would lead to highly variable rock compositions throughout the flow, depending on cumulate crystal proportions, whereas the three randomly analyzed rocks have very similar composition. In our experiments, olivine and Cr-rich spinel co-crystallize until about 18 wt% (about 23 volume %) olivine is formed, and then plagioclase and pigeonite join the crystallizing assemblage. Experimental results thus suggest that low-pressure crystallization will lead to early crystallization of about 23 volume % of olivine phenocrysts before crystallization of a pyroxene + plagioclase + olivine groundmass. Point-counting on microscopic images of the least altered of the Gusev basalts (Humphrey) indicates the presence of ~25 vol. % olivine megacrysts and pixels counts of grayscale images indicate ~20 volume % olivine megacrysts in a groundmass formed of pyroxene, plagioclase, chromite and phosphates (McSween *et al.*, 2006). This is in agreement with experimental results and supports the idea that olivine crystals in the Gusev basalts are not accumulated by crystal settling or added as xenocrysts. Furthermore, the composition of the olivine crystals at the point where pyroxene and plagioclase join the crystallizing assemblage is Fo_{68}, close to the Fo_{60} suggested by Mössbauer spectroscopy of Gusev basalts (Morris *et al.*, 2004).

4.2.2 Relation between Gusev basalts and olivine-phyric shergottites

Apart from the Gusev basalts, olivine-phyric shergottites (e.g. Goodrich, 2002; Greshake *et al.*, 2004) are the only known primitive basaltic rocks from Mars. When

compared to shergottites (including olivine-phyric shergottites), the Gusev basalts are enriched in Al_2O_3 and Na_2O (Figure 5), and have lower CaO/Al_2O_3 ratios (~0.7 compared to 1.1-1.9 for shergottites, Lodders, 1998). Olivine-phyric shergottites are also characterized by higher MgO contents (up to 21 wt%, Figure 5) and higher X_{Mg} (~0.66 for olivine-phyric shergottites, and ~0.50 for Gusev basalts). Although the similarities of Gusev basalts and olivine-phyric shergottites have been emphasized by some authors (e.g. McSween *et al.*, 2006), experimental results do not support such comparisons. Low-pressure crystallization of the Gusev basalts slightly modifies the Al_2O_3 content, but the residual liquids still do not evolve to the compositions of any of the olivine-phyric shergottites or other SNC meteorites (Figure 5). It does not appear, either, that Gusev basalts could have been derived from olivine-phyric shergottites through olivine and spinel crystallization. This scenario was modeled by calculating the effect on the Gusev bulk composition of adding back equilibrium proportions of olivine and spinel in 1% increments. This calculation was carried out to a final MgO content equal to that of Yamoto 980459 (18.1 wt %) and is shown in Figure 5. SiO_2, FeO, and Al_2O_3 all have significant discrepancies between the modeled value and the actual oxide value for Yamoto 980459. The experimental results thus indicate that shergottites cannot be related to the Gusev basalts by simple fractional crystallization, suggesting a different mantle source and/or different genetic processes.

The olivine-phyric shergottite Yamato 980459 (Y98, Greshake *et al.*, 2004), which contains the most magnesian olivines (Fo_{84}) of the Martian meteorites, is a good candidate for a primary mantle magma. Experimental work on Y98 shows that it is multiply saturated with olivine and orthopyroxene, with a multiple saturation pressure slightly higher than for the Gusev basalts (~1.2 GPa) and a higher temperature (1550 °C, Dalton *et al.*, 2005). The

magnesium-rich character of Y98 indicates that it may be from a more depleted mantle source than the iron-rich Gusev basalt composition. Thus, the class of olivine-phyric shergottites that are sampled as meteorites may represent a later remelting event that occurred in a mantle that had been depleted by an ancient melt extraction event. This would be in agreement with the young ages that have been proposed for shergottites (165-875 Ma, Jones, 1986; Nyquist *et al.*, 2001) compared to the old, Noachian, age of the Gusev basalts (Greeley *et al.*, 2005). The similarity between melts of a primitive Martian mantle composition noted above and the Gusev basalts are consistent with derivation of the Gusev magmas from a near-primitive Martian mantle composition.

4.2.3 Relation between Gusev basalts and the composition of the Martian crust

Experimental liquids obtained by low-pressure crystallization of Gusev basalts follow a tholeiitic differentiation trend (Figure 6) similar to that observed in Iceland or the Galapagos Spreading Center (Juster *et al.*, 1989). The liquid line of descent is characterized by a strong enrichment in FeO, with little variation in the SiO_2 content (Figure 6). Silica-rich rocks are difficult to obtain from such differentiation trends, and require very high degree of crystallization (e.g., Juster *et al.*, 1989). When compared to spectroscopically determined compositions of the Martian surface (surface types 1 and 2, McSween *et al.*, 2003), differentiation products of Gusev basalts have lower silica contents and higher FeO contents; differentiation does not lead toward the compositional field of surface types 1 or 2. This suggests that, under anhydrous conditions, Gusev basalts are not related to basaltic-andesite and andesite types 1 and 2 surface compositions.

The results raise the question of the relation of Gusev basalts to the primitive Martian crust. Rocks related to Gusev basalts are probably locally present in the primitive crust of the Southern Highlands, as strongly suggested by remotely-sensed spectroscopic data. Olivine-rich basalts are also present in crater floors of the Northern Plains (Bibring *et al.*, 2005). However, the bulk of the Martian crust probably originated from different magmatic processes.
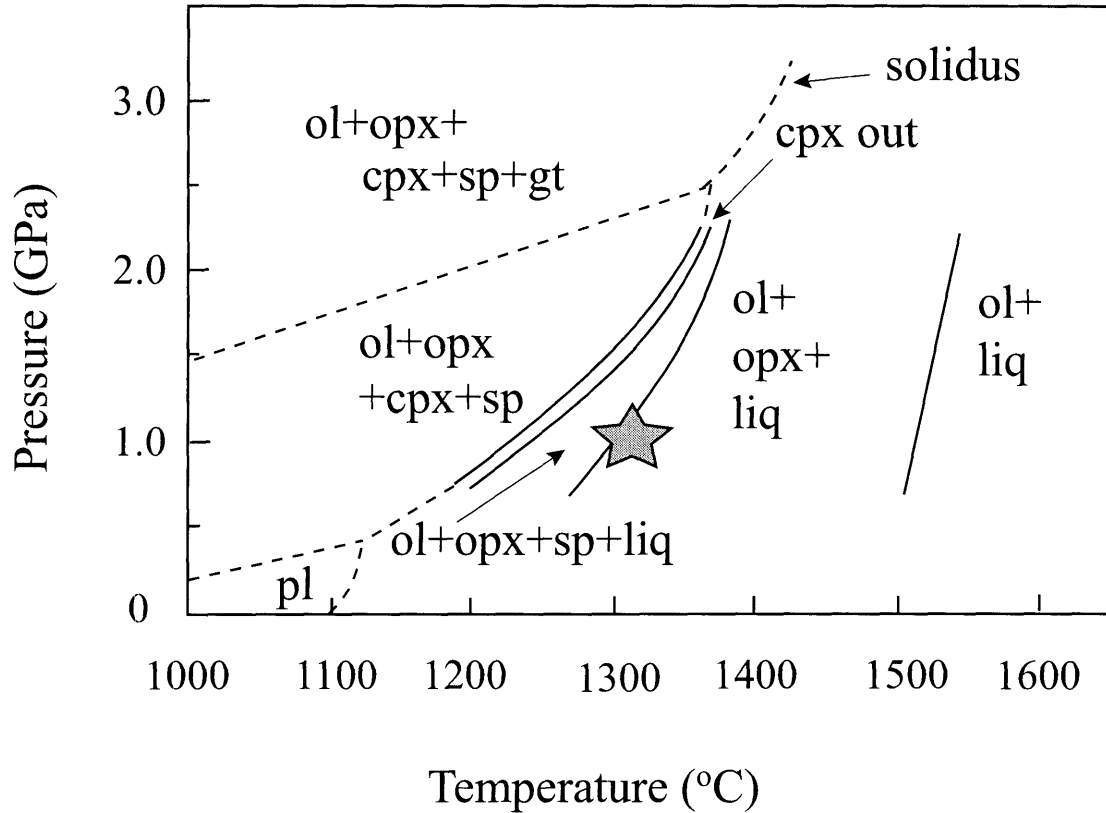
Figure 3. The Gusev composition (star) is multiply saturated with
olivine + opx + spinel at 1.0 GPa and 1310 °C. This corresponds well
with experiments done by Bertka and Holloway (1994a) on the Dreibus
and Wänke (1985) primitive martian mantle composition. Diagram
modified from Bertka and Holloway (1994a).
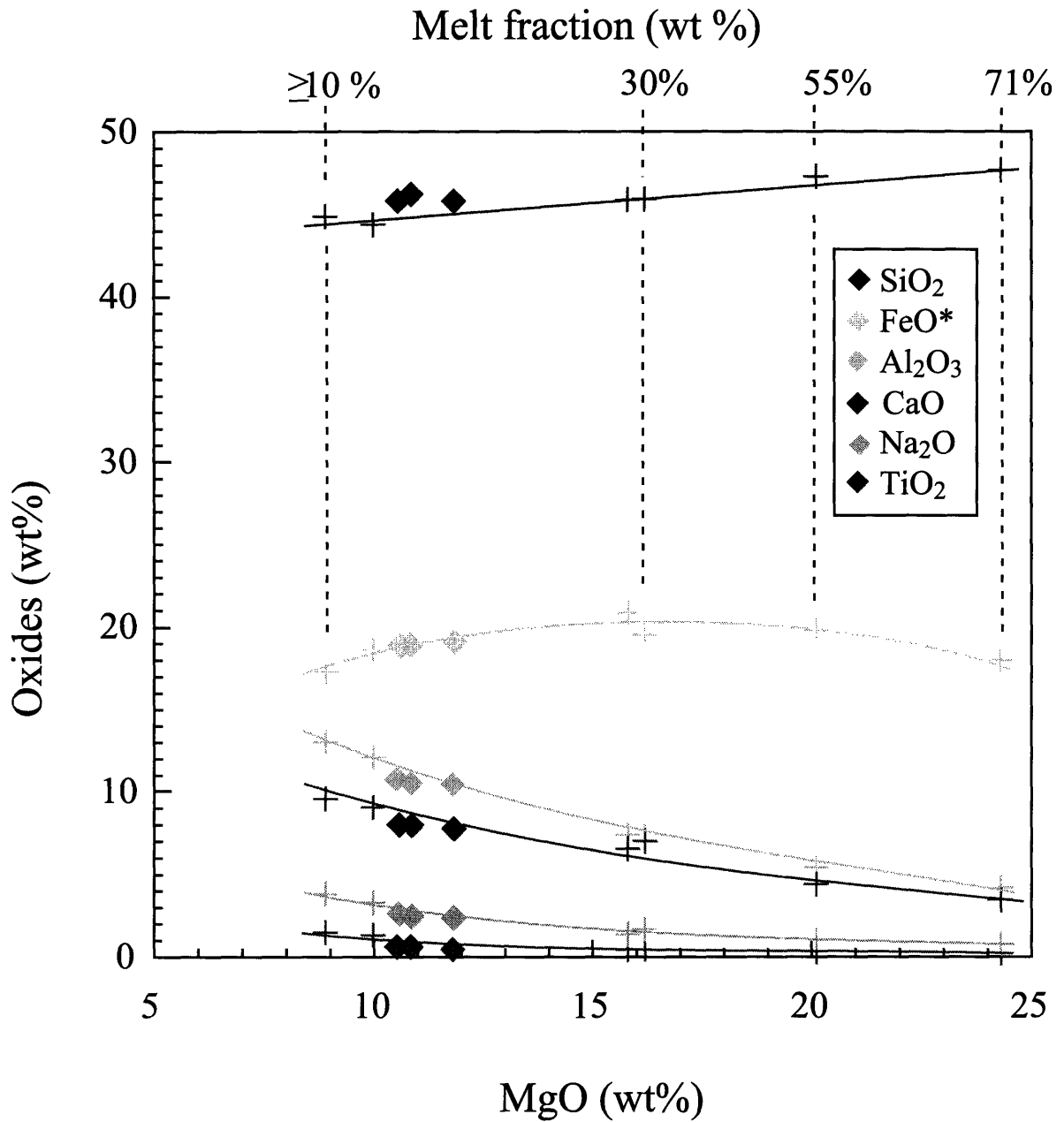
Figure 4. Comparison between the Gusev basalts (diamonds) and the
1.5 GPa experimental melting curves (Bertka and Holloway, 1994b) of the
Dreibus and Wänke (1985) primitive Martian mantle composition (crosses).
The Gusev basalts correspond to approximately a 15-20% melt of the
Martian mantle.
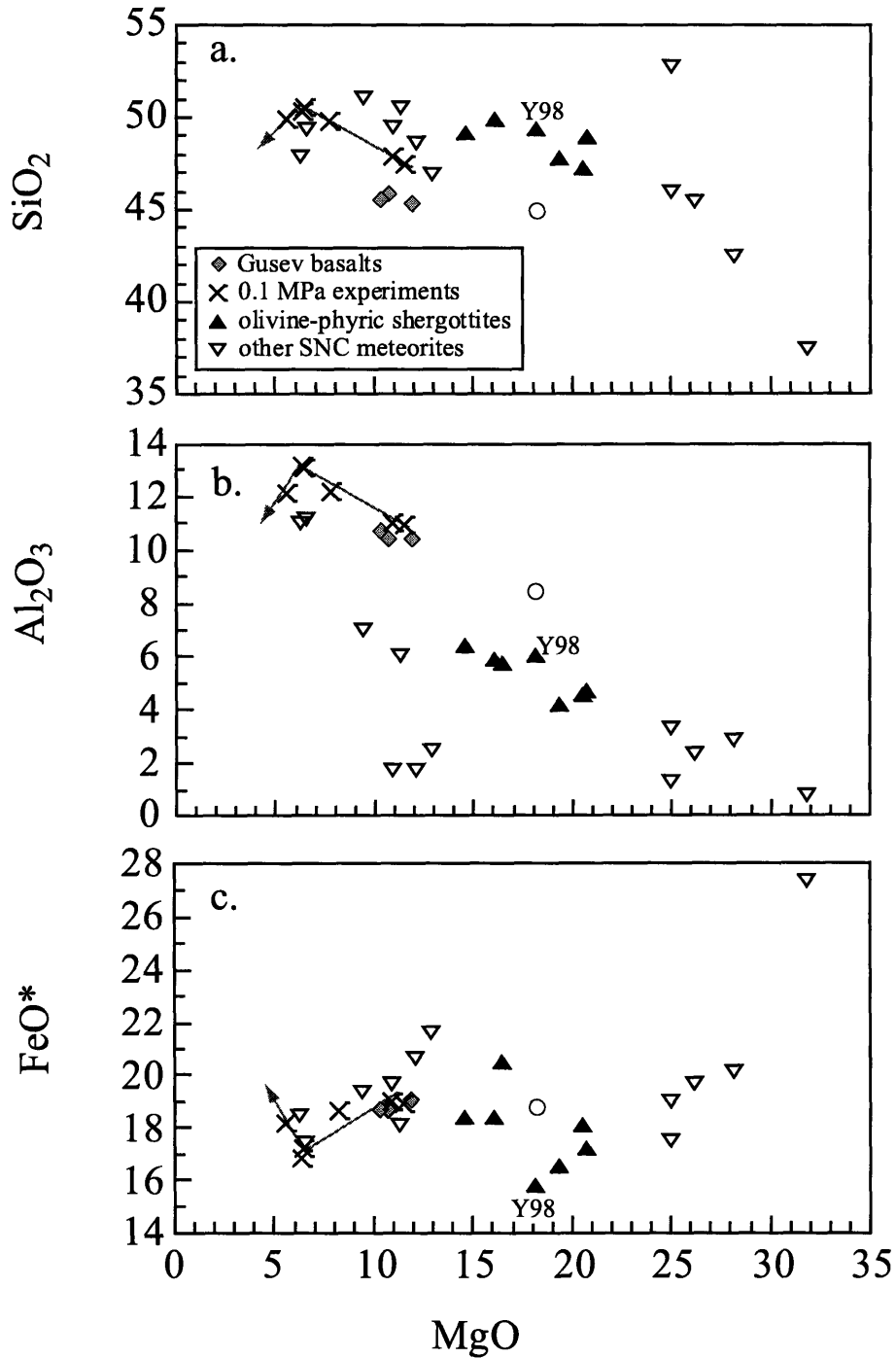
Figure 5. MgO vs. weight percent oxide for seven oxides. Low pressure crystallization (arrow) of the Gusev composition does not produce residual liquids similar to olivine-phyric shergottites (filled triangles) or other SNC meteorites (open triangles). The olivine-phyric shergottite Yamato 980459, discussed in the text, is identified on the figure as Y98. The open circle indicates the effect of adding back equilibrium proportions of olivine and spinel to the Gusev bulk composition to a final MgO content equal to that of Yamoto 980459.

Figure 5. (Continued from previous page)

Figure 6. Low-pressure experiments (X) on the recalibrated Gusev composition show that the Gusev basalts follow a tholeiitic (TH) fractionation path and will not produce liquids with a calc-alkaline (CA) surface type 1 or surface type 2 composition. Diagram modified from McSween et al. (2003).

Chapter 5

CONCLUSIONS

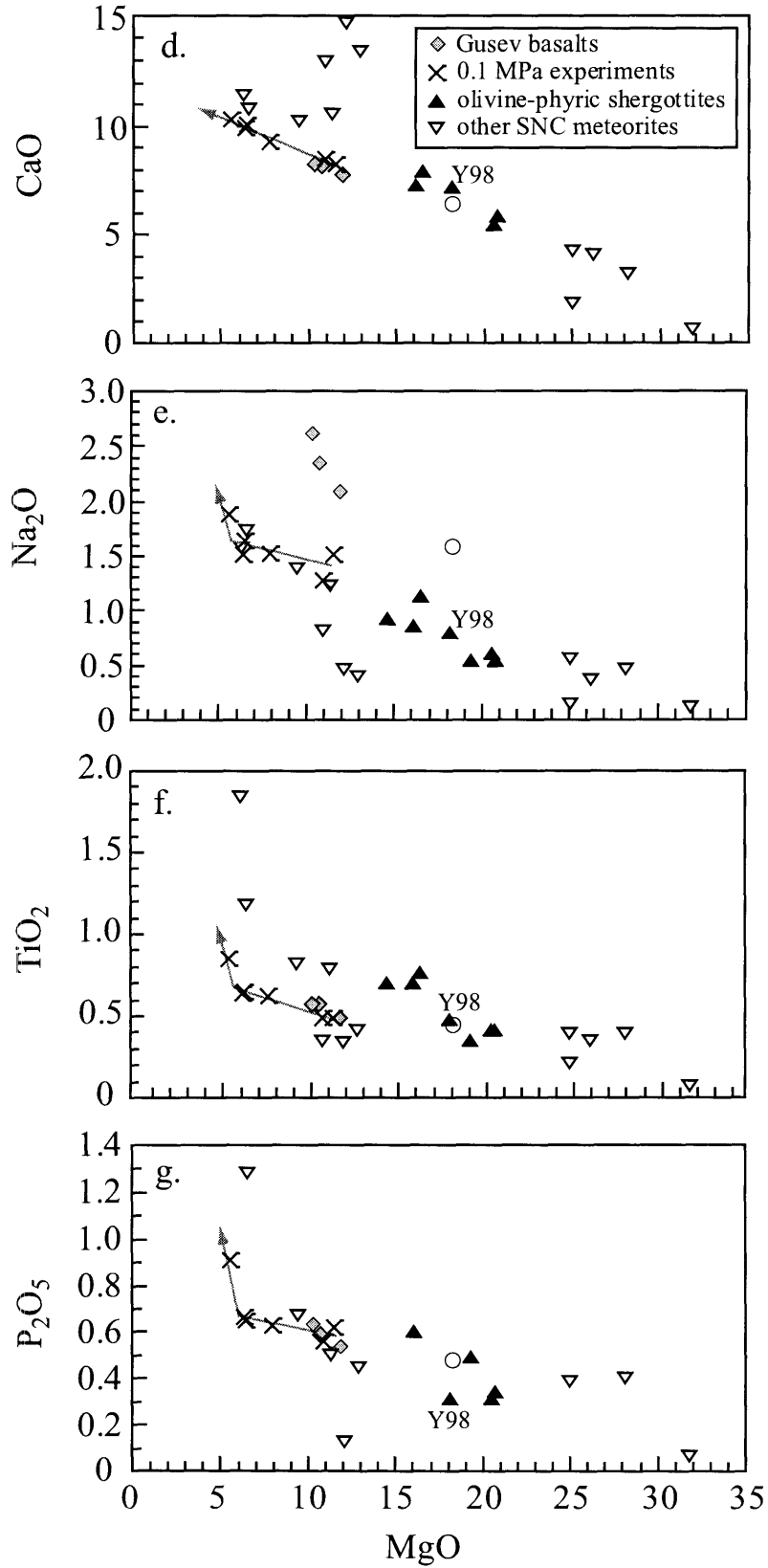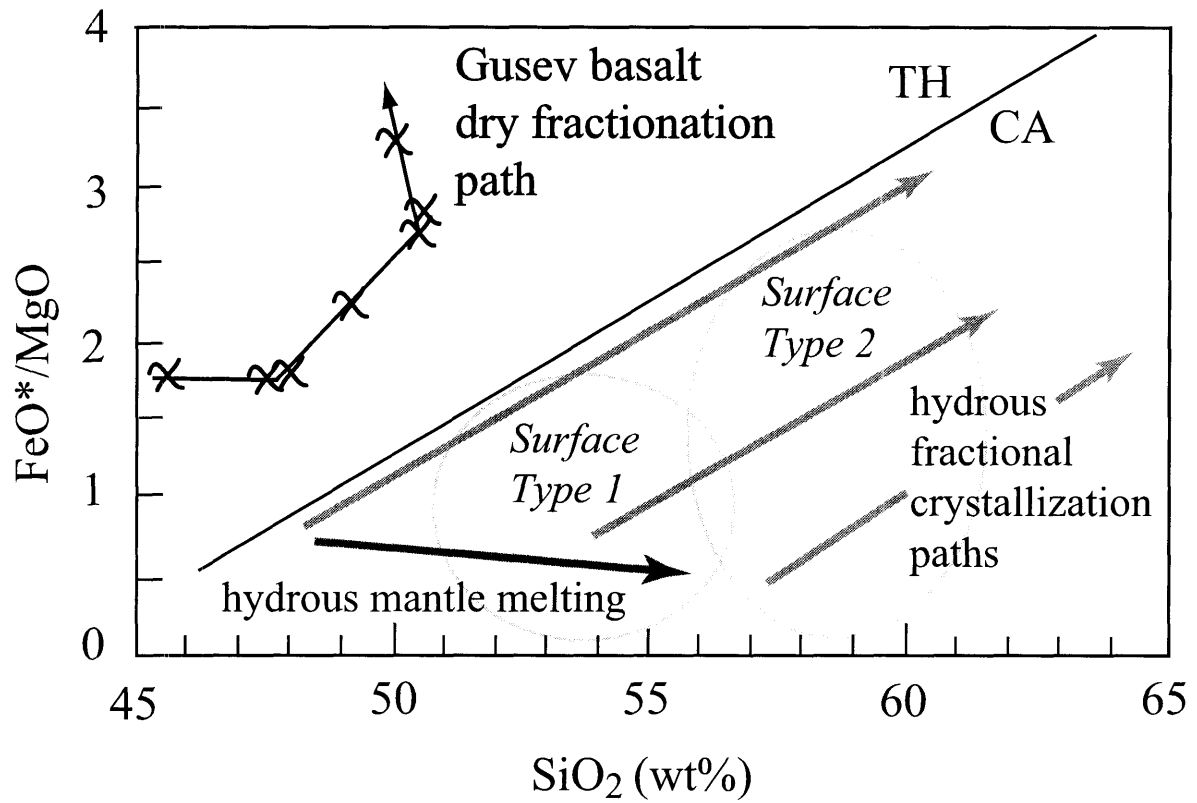Our experimental work suggests that the Gusev basalts from the Gusev crater plains are anhydrous near-primary melts that were last in equilibrium with the Martian mantle at 1310 °C and 85 km depth. Their composition is consistent with batch melting of a primitive Martian mantle at a melt fraction of 15 to 20%. Although Gusev basalts cannot be related to spectroscopically-determined surface compositions (TES surface types 1 and 2) through any low-pressure crystallization processes, similar olivine-rich basalts seem to be present throughout the Southern Highlands. Such rocks are indicative of high mantle potential temperatures on Mars during the Noachian era, maybe even until the very latest Noachian (3.6 Ga).

The Gusev basalts also do not appear to be related to olivine-phyric shergottites, which may represent melts from a depleted mantle source. Gusev basalts, on the other hand, are partial melts of a near-primitive Martian mantle, with a composition close to that estimated by Dreibus and Wänke (1985). Indeed, the existence of Gusev basalts support that this estimated composition is close to the actual composition of the Martian mantle.

Chapter 6

APPENDIX 1:

Experimental data on the preliminary Gusev composition

This study was begun on a starting composition that matched the initial rock compositions published for Adirondack, Humphrey, and Mazatzal (McSween et al., 2004). After our study was started, it was discovered that the sensor heads had been inadvertently switched at the launch site, requiring recalibration and recalculation of compositional data for the rocks. The results presented in this paper were based on experiments on the recalibrated composition. The data for the experiments performed on the preliminary composition are presented here for comparison. Table 1A compares the average preliminary and recalibrated composition from McSween et al. (2004) and McSween et al. (2006). MgO and FeO* increased and Na_2O decreased in the recalibrated composition, but the changes were generally less than 1 wt% absolute.

The experimental conditions and products for the preliminary composition are presented in Table 2A. For the initial composition, the experiments were multiply saturated with olivine, orthopyroxene, and spinel on the liquidus at 1.1 GPa and 1360 °C (Figure 1A), compared to 1.0 GPa and 1310 °C, but the phase relations stayed the same. Opx was still the first crystallizing silicate phase at pressures above multiple saturation, and olivine below. At 0.1 MPa, the appearance temperature for plagioclase and pigeonite was about 25 °C lower for the recalibrated composition. Compositional data for the preliminary dataset experiments are presented in Table 3A.
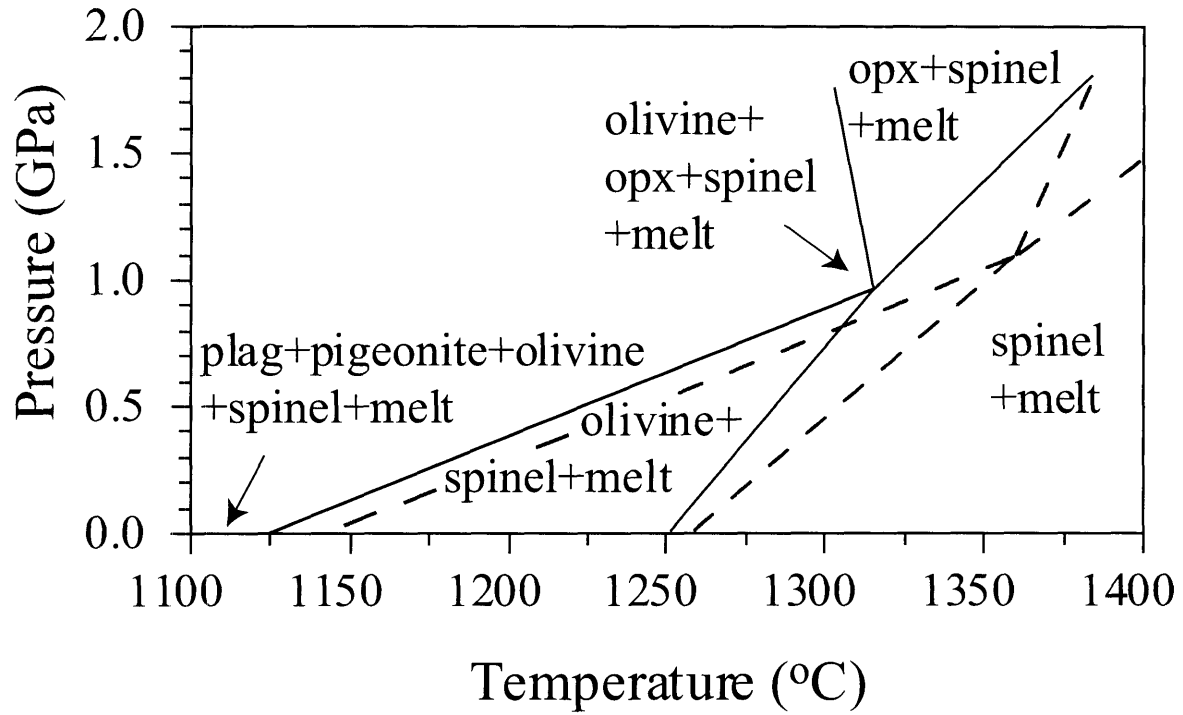
Figure 1A. Comparison of the experimentally determined phase relations for the preliminary (dashed lines) and recalibrated (solid lines) Gusev basalt composition. An olivine + orthopyroxene + spinel multiple saturation point was found on the liquidus near 1.0 GPa and 1310 °C for the recalibrated composition and at 1.1 GPa and 1360 °C for the preliminary composition.

44

Oxide (wt%)	Preliminary	Recalibrated
SiO_2	45.73	45.57
TiO_2	0.49	0.55
Al_2O_3	11.07	10.51
Fe_2O_3	2.60	3.03
Cr_2O_3	0.58	0.63
FeO	15.37	16.07
MnO	0.39	0.42
MgO	12.20	10.97
CaO	7.63	8.05
Na_2O	2.89	2.35
K_2O	0.06	0.08
P_2O_5	0.59	0.59
FeS	0.00	0.83
S	0.30	0.00
Total	99.91	99.64

Table 1A. Preliminary and recalibrated compositional data, representing an average of the compositions of Adirondack, Humphrey, and Mazatzal reported in McSween et al. (2006) and McSween et al. (2004)

Table 2A. Experimental conditions and products for preliminary Gusev composition

Run #	Pressure	Temp (°C)	Time (h)	Phases[a]	K_D ol/liq	K_D pyx/liq	K_D sp/liq	K_D pl/liq	Mg# gl	Mg# ol	Mg# pyx	Mg# sp	Ca# pl	ΣR^2	ΔFe
GUS-15	0.1 MPa	1125	123	ol (25) + pig (10) + plag (19) + sp (1) + gl (43)	0.35	0.30	1.92	0.74	0.37	0.63	0.67	0.24	0.68	0.56	0.38
GUS-3	0.1 MPa	1175	92	ol + sp + gl											
GUS-4	0.1 MPa	1200	73	ol (12) + sp (2) + gl (84)	0.31		1.58		0.49	0.76		0.38		0.69	-3.43
GUS-1	0.1 MPa	1250	24	ol + sp + gl											
GUS-2	0.1 MPa	1280	18	sp + gl											
GUS-5	1.0 GPa	1315	2	ol + opx + sp + gl											
GUS-6	1.0 GPa	1340	2.75	ol + opx + sp + gl											
GUS-11	1.0 GPa	1350	2.25	ol + sp + gl											
GUS-12	1.0 GPa	1370	3	sp + gl											
GUS-9	1.2 GPa	1355	2.25	ol + opx + sp + gl											
GUS-14	1.2 GPa	1375	2.5	sp + gl											
GUS-8	1.5 GPa	1380	2.25	opx + sp + gl											
GUS-10	1.5 GPa	1400	2.25	opx + sp + gl											
GUS-13	1.5 GPa	1420	2	sp + gl											

[a] Abbreviations and explanations as in Table 2

46

Table 3A. Electron microprobe analyses of phases produced in 0.1 MPa experiments on the preliminary Gusev composition

Run #	Phase[a]	SiO_2	TiO_2	Al_2O_3	Cr_2O_3	FeO	MnO	MgO	CaO	Na_2O	K_2O	P_2O_5	Total
0.1 MPa													
GUS-15	gl (12)	50.2 (6)	0.95 (8)	12.3 (2)	0.06 (2)	17.0 (4)	0.37 (3)	5.67 (14)	10.2 (1)	1.99 (10)	0.10 (1)	0.98 (12)	99.84
	ol (7)	36.6 (6)				32.3 (2)	0.60 (2)	30.2 (3)	0.41 (2)				100.09
	pig (7)	52.6 (3)	0.17 (2)	1.29 (5)	0.49 (2)	18.7 (3)	0.58 (2)	21.0 (5)	5.75 (67)	0.07 (3)			100.67
	pl (7)	52.1 (6)		29.3 (7)		1.23 (25)		0.38 (16)	13.6 (3)	3.53 (19)	0.04 (1)		100.18
	sp (7)	0.39 (18)	2.73 (75)	16.5 (1.6)	35.7 (4.1)	36.7 (2.2)	0.43 (2)	6.28 (31)	0.27 (4)				100.03
GUS-3	gl (9)	49.7 (2)	0.55 (5)	13.1 (1)	0.01 (1)	16.2 (1)	0.39 (3)	8.14 (6)	9.42 (4)	1.17 (6)	0.07 (1)	0.55 (6)	99.30
	ol (3)	37.8 (2)				23.0 (1)	0.46 (2)	38.5 (1)	0.40 (11)				100.05
	sp												
GUS-4	gl (9)	49.3 (3)	0.52 (5)	12.8 (1)	0.02 (3)	16.6 (2)	0.38 (3)	9.03 (13)	9.11 (8)	1.30 (9)	0.07 (1)	0.58 (6)	99.66
	ol (3)	38.5 (5)				22.1 (3)	0.39 (3)	38.8 (8)	0.29 (2)				100.02
	sp (3)	0.20 (15)	0.31 (4)	20.3 (3)	41.8 (8)	26.7 (2)	0.26 (4)	9.22 (22)	0.13 (4)				99.63
GUS-1	gl (9)	47.9 (3)	0.48 (6)	11.8 (1)	0.05 (2)	17.3 (2)	0.38 (3)	10.8 (1)	8.44 (9)	1.61 (7)	0.07 (1)	0.50 (4)	99.24
	ol (3)	38.3 (2)				20.1 (1)	0.40 (5)	41.7 (2)	0.31 (1)				100.79
	sp												
GUS-2	gl (9)	47.4 (2)	0.44 (3)	11.2 (1)	0.12 (2)	17.5 (2)	0.39 (2)	12.6 (1)	8.01 (10)	1.42 (10)	0.06 (1)	0.46 (5)	99.57
	sp												

[a]Abbreviations as in Table 2. Explanations as in Table 3.

REFERENCES

Agee C.B. and Draper D.S. (2004) Experimental constraints on the origins of the Martian mantle. *Earth and Planetary Science Letters*, 224: 415-429.

Armstrong J.T. (1995) CITZAF—A package of correction programs for the quantitative electron microbeam X-ray analysis of thick polished materials, thin-films, and particles. *Microbeam Analysis*, 4: 177-200.

Bertka C.M. and Holloway J.R. (1994a) Anhydrous partial melting of an iron-rich mantle I: subsolidus phase assemblages and partial melting phase relations at 10 to 30 kbar. *Contributions to Mineralogy and Petrology*, 115: 313-322.

Bertka C.M. and Holloway J.R. (1994b) Anhydrous partial melting of an iron-rich mantle II: primary melt compositions at 15 kbar. *Contributions to Mineralogy and Petrology*, 115: 323-338.

Bibring J.-P. et al. (2005) Mars surface diversity as revealed by the OMEGA/Mars Express observations. *Science*, 307: 1576-1581.

Biggar G.M. (1972) Diopside lithium metasilicate and the 1968 temperature scale. *Mineralogical Magazine*, 38: 768-770.

Boyd F.R. and England J.L. (1960) Apparatus for phase equilibrium studies at pressures up to 50 kilobars and temperatures up to 1,750 °C. *Journal of Geophysical Research*, 65: 741-748.

Brooker R., Holloway J.R. and Hervig R. (1998) Reduction in piston-cylinder experiments: The detection of carbon infiltration into platinum capsules. *American Mineralogist*, 83: 985-994.

Bryan W.B., Finger L.W. and Chayes F. (1969) Estimating proportions in petrographic mixing equations by least-squares approximation. *Science*, 163: 926-927.

Basaltic Volcanism Study Project (1981) *Basaltic Volcanism on the Terrestrial Planets.* Pergamon Press, Inc., New-York, 1286 pp.

Christensen P.R., Bandfield J.L., Smith M.D., Hamilton V.E. and Clark R.N. (2000) Identification of a basaltic component on the Martian surface from Thermal Emission Spectrometer data. *Journal of Geophysical Research*, 105: 9609-9621.

Dalton H.A., Musselwhite D.S., Kieffer W.S. and Treiman A.H. (2005) Experimental petrology of the basaltic shergottite Yamato 980459: Implications for the thermal structure of the Martian mantle. *Lunar and Planetary Science* [CD-ROM], *XXXVI*, abstract 2142.

Dreibus G. and H. Wänke (1984) Accretion of the Earth and the Inner Planets, 27th International Geological Congress, VNU Science Press, Moscow, pp. 1-20.

Dreibus G. and Wänke H. (1985) Mars, a volatile-rich planet. *Meteoritics,* 20: 367-381.

Elkins L.T., Fernandes V.A., Delano J.W. and Grove T.L. (2000) Origin of lunar ultramafic green glasses: Constraints from phase equilibrium studies. *Geochimica et Cosmochimica Acta,* 54: 2565-2574.

Gaetani G.A. and Grove T.L. (1998) The influence of water on melting of mantle peridotite. *Contributions to Mineralogy and Petrology,* 131: 323-346.

Gellert R., et al. (2006) Alpha Particle X-Ray Spectrometer (APXS): Results from Gusev crater and calibration report. *Journal of Geophysical Research, 111,* E02S05, doi: 10.1029/2005JE002555.

Ghiorso M.S. and Sack R.O. (1995), Chemical mass transfer in magmatic processes, IV. A revised and internally consistent thermodynamic model for the interpolation and extrapolation of liquid-solid equilibria in magmatic systems at elevated temperatures and pressures, *Contributions to Mineralogy and Petrology,* 119: 197-212.

Goodrich C.A. (2002) Olivine-phyric Martian basalts: a new type of shergottites. *Meteoritics and Planetary Science,* 37: B31-B34.

Greeley R., Foing B.H., McSween H.Y. Jr., Neukum G., Pinet P., van Kan M., Werner S.C., Williams D.A. and Zegers T.E. (2005), Fluid lava flows in Gusev crater, Mars. *Journal of Geophysical Research, 110,* E05008, doi: 10.1029/2005JE002401.

Greshake A. and Fritz J. Stöffler D. (2004) Petrology and shock metamorphism of the olivine-phyric shergottite Yamato 980459: evidence for a two-stage cooling and a single-stage ejection history. *Geochimica et Cosmochimica Acta,* 68: 2359-2377.

Grove T.L. (1981) Use of FePt alloys to eliminate the iron loss problem in 1-atmosphere gas mixing experiments: theoretical and practical considerations. *Contributions to Mineralogy and Petrology,* 78: 298-304.

Grove T.L. and Bence A.E. (1977) Experimental study of pyroxene-liquid interaction in quartz-normative basalt 15597. *Proceedings of the Lunar and Planetary Sciences Conference,* 8: 1549-1579.

Grove T.L. and Juster T.W. (1989) Experimental investigations of low-Ca pyroxene stability and olivine-pyroxene-liquid equilibria at 1-atm in natural basaltic and andesitic liquids. *Contributions to Mineralogy and Petrology,* 103: 287-305.

Halliday, A. N., Wänke H., Birck J.-L. and Clayton R. N. (2001), The accretion, composition and early differentiation of Mars. *Space Science Reviews,* 96: 197-230.

Hamilton V.E. and Christensen P.R. (2005) Evidence for extensive olivine-rich bedrock on Mars. *Geology,* 33: 433-436.

Hays (1966) Lime-alumina-silica. *Carnegie Institution of Washington Yearbook,* 65: 234-236.

Hoefen T.M. et al. (2003) Discovery of olivine in the Nili Fossae region of Mars. *Science,* 302: 627-630.

Johannes W., Chipman D.W., Hays J.F., Bell P.M., Mao H.K., Newton R.C., Boettcher A.L. and Seifert F. (1971) An interlaboratory comparison of piston cylinder pressure calibration using the albite-breakdown reaction. *Contributions to Mineralogy and Petrology,* 32: 24-38.

Jones J.J. (1986) A discussion of isotopic systematics and mineral zoning in the shergottites: Evidence for a 180 m.y. igneous crystallization age. *Geochimica et Cosmochimica Acta,* 50: 969-977.

Juster T.C., Grove T.L. and Perfit M.R. (1989) Experimental constraints on the generation of FeTi basalts, andesites, and rhyodacites at the Galapagos spreading center, 85° W and 95° W. *Journal of Geophysical Research,* 94: 9251-9274.

Kinzler R.J. and Grove T.L. (1992) Primary magmas of mid-ocean ridge basalts 2. Applications. *Journal of Geophysical Research,* 97: 6907-6926.

Lindsley D.H., Kesson S.E., Hartzman M.J. and Cushman M.K. (1974) The stability of armalcolite: experimental studies in the system Mg-Fe-Ti-O. *Proceedings of the Lunar and Planetary Sciences Conference,* 5: 521-534.

Lodders, K. (1998) A survey of shergottite, nakhlite and chassigny meteorites whole-rock compositions. *Meteoritics and Planetary Science,* 33: A183-A190.

McKenzie D. and Bickle M.J. (1988) The volume and composition of melt generated by extension of the lithosphere. *Journal of Petrology,* 29: 625-679.

McSween H. Y. Jr. (2002) The rocks on Mars, from far and near. *Meteoritics and Planetary Science,* 37: 7-25.

McSween H.Y. Jr., Grove T.L. and Wyatt M.B. (2003) Constraints on the composition and petrogenesis of the Martian crust. *Journal of Geophysical Research,* 108, E12, 5135, doi: 10.1029/2003JE002175.

McSween H.Y. et al. (2004) Basaltic rocks analyzed by the Spirit rover in Gusev Crater. *Science,* 305: 842-845.

McSween H.Y. et al. (2006) Characterization and petrologic interpretation of olivine-rich basalts at Gusev Crater, Mars. *Journal of Geophysical Research, 111*, E02S10, doi: 10.1029/2005JE002477.

Minitti M.M. and Rutherford M.J. (2000) Genesis of the Mars Pathfinder "sulfur-free" rock from SNC parental liquids. *Geochimica et Cosmochimica Acta,* 64: 2535-2547.

Monders A.G., Médard E. and Grove T.L. (2005) Primary Martian Basalts at Gusev Crater: Experimental Constraints. *Lunar and Planetary Science* [CD-ROM], *XXXVI*, abstract 2069.

Morris R. V. et al. (2004) Mineralogy at Gusev Crater from the Mössbauer spectrometer on the Spirit rover. *Science,* 305: 833-836.

Mustard J.-F. et al. (2005) Olivine and pyroxene diversity in the crust of Mars. *Science,* 307: 1594-1597.

Nyquist L.E., Bogard D.D., Shih C.-Y., Greshake A., Stöffler D. and Eugster O. (2001) Ages and geologic histories of Martian meteorites. Space Science Reviews 96: 105-164.

Putirka K., Johnson M., Kinzler R.J., Longhi J. and Walker D. (1996) Thermobarometry of mafic igneous rock based on clinopyroxene-liquid equilibria, 0-30 kb. *Contributions to Mineralogy and Petrology,* 123: 92-108.

Sanloup C., Jambon A. and Gillet P. (1999) A simple chondritic model of Mars. *Physics of the Earth and Planetary Interiors,* 112: 43-54.

Squyres, S.W. et al. (2006), Rocks of the Columbia Hills. *Journal of Geophysical Research,* 111(E2), E02S11, doi: 10.1029/2005JE002562.

Tormey D.L., Grove T.L. and Bryan W.B. (1987) Experimental petrology of normal MORB near the Kane Fracture Zone: 22° – 25° N, mid-Atlantic ridge. *Contributions to Mineralogy and Petrology,* 96: 121-139.

Wagner T.P. and Grove T.L. (1997) Experimental constraints on the origin of lunar high-Ti ultramafic glasses. *Geochimica et Cosmochimica Acta,* 61: 1315-1327.

Watson E.B. (1987) Diffusion and solubility of Pt in C. *American Mineralogist,* 72: 487-490.

Zuber M.T. et al. (2000) Internal structure and early thermal evolution of Mars from Mars Global Surveyor topography and gravity. *Science, 287,* 1788-1793.